Constraining U.S. ammonia emissions using TES remote sensing observations and the GEOS-Chem adjoint model

L. Zhu[1], D. K. Henze[1], K. E. Cady-Pereira[2], M. W. Shephard[3,4], M. Luo[5], R.W., Pinder[6], J. O. Bash[6], G. Jeong[1,6]

[1]Department of Mechanical Engineering,

Abstract.

Ammonia (NH_3) is an important contributor to air pollution, and it also has significant impacts on climate change and environmental health. However, there are many uncertainties in ammonia emissions inventories, from the total amount of emissions to the seasonal and diurnal variability, which hinder the use of air quality models to address these issues. In this paper,

University of Colorado, Boulder, Colorado, USA.

[2]Atmospheric and Environmental Research, Inc., Lexington, Massachusetts, USA.

[3]Atmospheric and Climate Application, Inc., East Gwillimbury, ON, Canada.

[4]Environment Canada, Toronto, Ontario, Canada.

[5]Jet Propulsion Laboratory, California Institute of Technology Pasadena, CA, USA.

[6]US Environmental Protection Agency, Research Triangle Park, North Carolina, USA.

we constrain ammonia emissions in the U.S. by assimilating observations from the TES remote sensing instrument with the GEOS-Chem model and its adjoint at 2°×2.5° horizontal resolution. This inversion framework is first validated using simulated observations. We then proceed to assimilate TES observations for April, July and October of 2006 through 2009. The inverse modeling results are evaluated by comparing the observationally constrained model simulations to independent surface measurements of NH_3, NH_x (NH_4^+ + NH_3) wet deposition, and SO_4^{2-} and NO_3^- aerosol. Modeled NH_3 concentrations have a decreased bias in April and October compared to surface observations after assimilation and an increased correlation in each month. Modeled NH_x wet deposition after assimilation has a decreased normalized mean bias (NMB) in April and an increased NMB in July and October compared to the wet NH_x observations, although the correlation and linear regression coefficients are closer to unity in each month. Modeled SO_4^{2-} and NO_3^- aerosols concentrations do not change significantly and persistent NO_3^- overestimation is noted, consistent with previous studies. Overall, assimilation of NH_3 remote sensing data to constrain NH_3 emissions improves the model simulation in several aspects, yet additional work on assessing wet deposition at a higher horizontal resolution, nitric acid formation, and bi-directional fluxes may be necessary to enhance model performance across the full range of gas and aerosol evaluations.

1. Introduction

Emissions of ammonia (NH_3) from anthropogenic sources pose several environmental concerns. Ammonia affects air quality and climate through its role in the mass, composition and physical properties of tropospheric aerosol. Ammonium nitrate and ammonium sulfate make up a substantial fraction of atmospheric fine particulate matter ($PM_{2.5}$), exposure to which has been statistically associated with inhibited lung development, cardiovascular diseases and premature mortality [*Pope et al.*, 2002; *Schwartz et al.*, 2002; *Reiss et al.*, 2007]. These fine particulates ($PM_{2.5}$) also contribute to haze that impacts visibility. Further, when deposited in excess, reactive nitrogen, including ammonia, can cause detrimental nutrient imbalances to sensitive ecosystems [*Rodhe et al.*, 2002; *Rabalais*, 2002].

Despite the recognized importance of NH_3 emissions in the U.S. [*Aneja et al.*, 2008], knowledge of their magnitude is severely limited; NH_3 emissions are primarily from agricultural sources whose strengths are difficult to characterize. Uncertainty in NH_3 undermines the efforts to understand historical and present levels of $PM_{2.5}$ [*Yu et al.*, 2005; *Nowak et al.*, 2006; *Zhang et al.*, 2008; *Wu et al.*, 2008; *Stephen and Aneja*, 2008; *Beusen et al.*, 2008; *Simon et al.*, 2008; *Henze et al.*, 2009] and hinders estimates of the response of $PM_{2.5}$ to control measures because of the key role that NH_3 plays in governing the balance of inorganic fine particulate species [*Dennis et al.*, 2008]. Model estimates of inorganic $PM_{2.5}$ have been compared to surface measurements [*Park et al.*, 2004, 2006; *Liao et al.*, 2007; *Henze et al.*, 2009; *Pye et al.*, 2009] and measurements from aircraft campaigns [*Heald et al.*, 2005, 2006]; NH_3 emissions are frequently indicated to be a likely cause of

discrepancies. On a larger scale, NH_3 emissions rates are a critical source of uncertainty in global budgets of the atmospheric transport and deposition of reactive nitrogen [*Sutton et al.*, 2007; *Galloway et al.*, 2008; *Schlesinger*, 2009].

These are several reasons for the persistence of uncertainties in NH_3 inventories. Characterizing NH_3 sources from the bottom up requires spatially and temporally resolved data such as detailed farming practices and intensity. These data are rarely available nationally as direct measurements of NH_3 emissions at such scales are prohibitive owing to cost. Therefore, people have turned to top-down approaches to provide additional constraints on NH_3 emissions estimates. While direct observations of gas-phase NH_3 do exist in select locations, observations of other chemically related species are much more prevalent. Further, NH_3 can rapidly partition to form aerosol ammonium (NH_4^+) which can limit the utility of gas-phase observations alone.

Consequently, owing to the paucity of direct observations of NH_3 and the difficulty of constraining the NH_x (= NH_3 + NH_4^+) system, measurements of species that are regulated by the amount of available NH_3 have been looked to for constraints on estimates of NH_3 emissions. The current National Emissions Inventory (NEI) for NH_3 is coarsely constrained by top-down estimates from the inverse modeling studies of *Gilliland et al.* [2003, 2006]. Measurements of wet deposited NH_x were used as constraints, because wet deposited NH_x estimates depend less than NH_3 on model sensitivity to aerosol partitioning. A drawback to this approach is the sensitivity to estimated precipitation and scavenging, aspects which are difficult to model accurately and hinder the inversion during some seasons. Taking an alternative approach, *Henze et al.* [2009] used measurements of SO_4^{2-} and NO_3^- from the IMPROVE network to constrain the amount of NH_3 partitioned

into the aerosol phase as NH_4^+ (which is strongly coupled to SO_4^{2-} and NO_3^-). In this way, aerosol-phase observations were used to constrain NH_3 concentrations and, hence, NH_3 emissions. This approach, however, is susceptible to model bias in HNO_3, which may be significant [*Zhang et al.*, 2012].

Despite these recent efforts, comparisons between inverse modeling results to the recent bottom-up NH_3 inventory of *Pinder et al.* [2006] show that considerable disagreements remain in the spatial and seasonal distribution of NH_3 emissions throughout the U.S. [*Henze et al.*, 2009]; at odds are estimates of the relative magnitude of spring vs summer emissions. A limiting factor in reconciling these differences is infrequent and sparse in situ observations, even for the aerosol-phase measurements, and a shortage of direct constraints on gas-phase NH_3. Without understanding the NH_x system as a whole, and without tools to link observations of these species over the continent to emissions, studies of NH_3 or NH_4^+ alone may suffer in terms of utility for constraining emissions inventories at a national scale [*Pinder et al.*, 2006].

The detection of boundary layer ammonia from space [*Beer et al.*, 2008; *Clarisse et al.*, 2009, 2010; *Shephard et al.*, 2011] provides a new and unprecedented opportunity for reducing persistent uncertainties in our understanding of the distribution and impacts of atmospheric ammonia. Initial comparisons to global model NH_3 distributions indicate that NH_3 sources may be widely underestimated [*Clarisse et al.*, 2009; *Shephard et al.*, 2011]. *Pinder et al.* [2011] have recently verified the utility of such measurements for tracking observed spatial and temporal trends in surface level NH_3 concentrations. Therefore, we consider here how inverse modeling with assimilation of satellite observations of NH_3 can be used to further provide constraints on NH_3 sources. Section 2 describes the models

and inverse methodology used in this study. We then present details of the remote sensing observations (Section 3), followed by inverse modeling tests using simulated observations (Section 4), and real observations (Section 5). Finally, we evaluate the modeled results by comparing them to independent data sets which are not used during the inversion (Section 6) and present our conclusions (Section 7).

2. Methods

2.1. GEOS-Chem

GEOS-Chem is a chemical transport model driven with assimilated meteorology from the Goddard Earth Observing System (GEOS) of the NASA Global Modeling and Assimilation Office [*Bey et al.*, 2001]. The tropospheric oxidant chemistry simulation in GEOS-Chem includes a detailed ozone-NO_x-hydrocarbon chemical mechanism of 80 species and over 300 reactions [*Bey et al.*, 2001]. GEOS-Chem includes an online secondary inorganic aerosol simulation introduced and described in full by *Park et al.* [2004]. Global anthropogenic sources and natural sources of NH_3 are from the 1990 GEIA inventory [*Bouwman et al.*, 1997]. As described in *Park et al.* [2004], the yearly total U.S. NH_3 emissions are scaled to match that of *Gilliland et al.* [2003], with seasonality based on temperature for animals and soils [*Aneja et al.*, 2000; *Roelle and Aneja*, 2002] and daylight [*Adams et al.*, 1999] for crops and fertilizers. The biomass burning and biofuel use are from inventories by *Duncan et al.* [2003] and *Yevich and Logan* [2003].

2.2. GEOS-Chem adjoint model

The adjoint model is an efficient method for calculating the gradient of a scalar model response function with respect to all of the model parameters simultaneously. The adjoint

of the GEOS-Chem model was developed specifically for inverse modeling of precursors of inorganic $PM_{2.5}$ with explicit inclusion of gas-phase chemistry, heterogeneous chemistry, and treatment of the thermodynamic couplings of the sulfate - ammonium - nitrate - water aerosol system [*Henze et al.*, 2007, 2009]. As the only adjoint model to explicitly represent this system, it is uniquely capable of assimilating speciated measurements of both gaseous and particulate components using the 4D-Var method [*Sandu et al.*, 2005]. The accuracy of the adjoint model calculations is verified through extensive comparisons of adjoint to finite difference sensitivities. In order to maximize points of comparison between these two approaches, we consider both ensembles of 1-D models (i.e., no horizontal transport) as well as spot tests of the full 3-D adjoint model (testing the full adjoint model for each parameter is not feasible, as it would require separate forward model calculations for each of the approximately 10^5 parameters). Fig. 1 shows the results of a week-long test of the sensitivity of surface level aerosol nitrate in each model column to NH_3 emissions in that column, demonstrating the accuracy of the adjoint gradient calculation.

2.3. Inverse modeling

Data assimilation techniques provide a framework for combining observations and models to form an optimal estimation of the state of a system, which in this case is the chemical makeup of the troposphere. To start with, a range of parameters are typically constructed using control variables, $\boldsymbol{\sigma}$, to adjust elements of the vector of model parameters, $\mathbf{p}$, via application as scaling factors, $p = p_a e^{\sigma}$, where $\mathbf{p_a}$ is the prior parameter estimate. The approach we consider iteratively employs the adjoint of an air quality model in a method referred to as 4D-Var, used here for inverse modeling of emissions. The advantage of this method is that numerous ($\mathcal{O}(10^5)$) model parameters can be optimized simultaneously

while still retaining the constraints of the full forward model physics and chemistry. This approach to inverse modeling seeks $\boldsymbol{\sigma}$ that minimizes the cost function, $\mathcal{J}$, given by

$$\begin{aligned}\mathcal{J} &= \frac{1}{2}\sum_{\mathbf{c}\in\Omega}(H\mathbf{c}-(\mathbf{c}_{obs}-\mathbf{b}))^T\mathbf{S}_{obs}^{-1}(H\mathbf{c}-(\mathbf{c}_{obs}-\mathbf{b})) \\ &+ \frac{1}{2}\gamma(\boldsymbol{\sigma}-\boldsymbol{\sigma}_a)^T\mathbf{S}_a^{-1}(\boldsymbol{\sigma}-\boldsymbol{\sigma}_a) \qquad (1)\end{aligned}$$

where H is the observation operator, γ is the regularization parameter, $\boldsymbol{\sigma}_a$ is the prior estimate of the control variables, $\mathbf{S}_a$ and $\mathbf{S}_{obs}$ are error covariance estimates of the control variables and observations respectively, and Ω is the domain over which observations, $\mathbf{c}_{\rm obs}$, and model predictions are available, and $\mathbf{b}$ is a bias correction explained in section 5. Overall, the cost function is a specific model response, the minimum value of which balances the objectives of improving model performance while ensuring the model itself remains within a reasonable range (as dictated by $\mathbf{S}_a^{-1}$) of the initial model. Gradients of the cost function with respect to the parameter scaling factors calculated with the adjoint model, $\nabla_{\boldsymbol{\sigma}}\mathcal{J}$, are supplied to an optimization routine (the quasi-Newton L-BFGS-B optimization routine *Byrd et al.* [1995]; *Zhu et al.* [1994]), and the minimum of the cost function is sought iteratively. At each iteration, improved estimates of the model parameters are updated and the forward model solution is recalculated.

3. Observations

3.1. Remotely sensed NH_3 observations from TES

The high spectral resolution and good signal-to-noise ratio of the TES instrument [*Shephard et al.*, 2008] have enabled the first detection of tropospheric ammonia from space, first demonstrated over Southern California and China [*Beer et al.*, 2008]. TES is an infrared Fourier transform spectrometer with spectral resolution of 0.06 $\rm cm^{-1}$ aboard the

NASA Aura satellite, launched July 15, 2004 [*Schoeberl et al.*, 2006]. TES global survey observations repeat with a 16-day cycle and have a nadir footprint of 5 km × 8 km; for example, that is about ∼180 daytime retrievals a month over North America after cloud screening (optical depths < 1.0) and applying the TES retrieval quality control flags.

Comparison of model estimates to satellite observations is done via application of the following formula for the TES observational operator, H,

$$H\mathbf{c} = \mathbf{c}_a + \mathbf{A}(\mathbf{M}\mathbf{c} - \mathbf{c}_a) \quad (2)$$

where $\mathbf{c}$ is the model estimated NH_3 profile, $\mathbf{M}$ is a matrix that maps these values to the retrieval units and vertical levels, $\mathbf{A}$ is the averaging kernel, and $\mathbf{c}_a$ is the a priori NH_3 profile used for the retrieval [*Shephard et al.*, 2011]. By comparing TES NH_3 profiles to mapped model estimates, $H\mathbf{c}$, rather than the native model NH_3 profile, $\mathbf{c}$, the contribution of error in $\mathbf{c}_a$ to the measurement error, $\mathbf{S}_{obs}$, is minimized [*Rodgers*, 2000].

For the sake of 2D visualization, the Representative Volume Mixing Ratio (RVMR) metric [*Payne et al.*, 2009; *Shephard et al.*, 2011] is used in this study to provide a means of comparing TES profiles to model estimates in a manner that accounts for heterogeneity in the instrument's sensitivity to NH_3.

3.2. Surface measurements

In this study, model estimates are evaluated using surface observations of ammonia, sulfate, nitrate, ammonium and wet deposited NH_x from several monitoring networks throughout the U.S.. Surface NH_3 observations are from the National Atmospheric Deposition Program (NADP) Ammonia Monitoring Network (AMoN), which is comprised of triplicate passive ammonia monitoring samplers located at 21 sites across the U.S. with

a two-week long sample accumulation. The locations of these 21 monitoring stations are shown in Fig. 2. Observations from each site are compared with modeled concentrations during the year November 2007 through June 2010.

Wet deposition observations are taken from the NADP National Trends Network (NTN) (http://nadp.sws.uiuc.edu/NADP), which are predominantly located away from urban areas and point sources of pollution. NTN has more than 200 sites with week-long sample accumulation.

Model estimates of sulfate and nitrate aerosols are compared to observations from the Interagency Monitoring of Protected Visual Environments (IMPROVE) network for the year 2008 [*Malm et al.*, 2004]. The IMPROVE network collects $PM_{2.5}$ particles on Teflon, nylon, and quartz filters using a modular, cyclone-based sampler with critical orifice flow control. Sulfate and nitrate aerosols are collected on nylon filters, which are sampled over 24 h every third day.

4. Pseudo inversions

We first assess the capabilities and limitations of the GEOS-Chem inverse modeling setup in idealized control conditions by designing inverse problems with known solutions. Pseudo-observations are generated through application of the TES NH_3 retrieval algorithm [*Shephard et al.*, 2011] to a simulated atmosphere from GEOS-Chem. The emissions used during this simulation are designated as the true emissions. Sampling times, locations and error estimates reflect those of actual TES observations although retrieval bias ($\mathbf{b}$) is not included in these tests. For these tests, 87 pseudo TES observations are used from July 14 through 19, 2005, along roughly a dozen global survey transects crossing the midwestern U.S..

To test the inverse model, NH_3 emissions parameters were initialized to values different from the true emissions. In the first test, initial model emissions are half of the true value. Fig. 3(a) shows these values in black along with linear line slope m and r^2. After optimization, the recovered emissions are unbiased and have a visible variance around the true emissions of ∼30%, as shown in blue in Fig. 3(a). In a second test using the same pseudo observations, the model emissions were initially biased high by a factor of 1.8 (Fig. 3(b)). The emissions recovered after optimization have a 20% high bias and again a 30% variance about the true values. While the variance of the recovered emissions is similar in both tests, the inversion starting with emissions that are initially too high is less successful.

To further investigate the reasons for this asymmetry and the variance of the optimized emissions, additional tests are performed to separate the possible impacts of inversion error, retrieval bias and measurement error. In each of the following tests, the true emissions are used to initialize the inversion. The first test uses the same pseudo observations as previously generated. This test again results in a high bias. As the same model state is used to generate the pseudo observations as was used to intialize the inversion, this bias can be attributed to a high bias in the retrieval itself. Retrieval bias, as explained further in *Shephard et al.* [2011], is owing to the fact that the retrieval always selects a moderate or polluted profile as an initial guess in order to avoid the null space of the radiative transfer operator. As the optimal estimation algorithm iterates towards a solution, the process may halt when values reach TES's detection threshold, resulting in a high bias. To test this, the retrieval algorithm is modified to use only a moderate profile as an initial guess. Pseudo observations generated using these profiles lead to slightly less high bias in the

inversion, at the cost of increased variance, see Fig. 4(b). As the magnitude of the final bias in tests whose results shown in (a) and (b) are similar to those in the pseudo inversions, it seems that the retrieval bias explains the bias exhibited in the pseudo inversions, and thus the entire process of inverting for NH_3 emissions is not appreciably intrinsically biased. To isolate the impact of measurement noise, the model profiles from the true model are applied with the same size error as the measurement error, and then assimilated. These profiles, unlike the previous tests, correspond directly to the true model and are not retreived profiles from the retrieval process. The impact of this measurement noise is only a slight adjustment in the emissions. Thus, the variance exhibited in the pseudo inversions is intrinsic to the inversion process itself, and would occur even if observations were perfect. This happens because there are variations in emissions that lie in the null space of the forward model. In other words, having some emissions too high and some emissions too low can result in indistinguishable (to TES) distributions of NH_3. Overall, the pseudo observation tests lead us to conclude that (1) measurement noise alone will not lead to unstable inversions (2) emissions that are underestimated can likely be recovered (3) emissions that are overestimated will be decreased, though this is countered by bias in the retrievals leading to overestimate of emissions in conditions where the model emissions are intially too high and (4) that many more iterations and observations would be necessary to reduce the variance of the emissions estimates from the truth, which will be at best $\sim$30%. While substantial, this is a significant improvement over initial errors of $\sim$100%. Although between points (2) and (3) is likely owing to the larger magnitude of the bias for retrievals with larger values (see Supplementary Figure 1).

5. TES assimilation

We next proceed to constrain U.S. NH_3 sources using real observations. TES observations throughout 2006 - 2009 are compared to model estimates from a 2008 GEOS-Chem global $2^\circ \times 2.5^\circ$ simulation. Four years of observations are necessary to provide sufficient spatial data coverage. Inter-annual comparisons of monthly AMoN NH_3 data indicate no substantial trends in this time period.

Thousands of TES retrievals are available for the assimilation, but not all of the TES retrievals are usable. The satellite can not always detect NH_3 for several reasons, such as the presence of clouds, low NH_3 concentrations (low signal to the noise ratio), and poor thermal contrast between the earth and atmosphere. Thus quality and diagnostic flags are defined to classify and filter the retrievals, keeping only those that have Degree Of Freedom For Signal (DOFS) greater than 0.1, or DOFS less than 0.1 but with high (absolute value greater than 7 K) thermal contrast. We use the retrievals from daytime only as the retrievals at night time do not appear to capture the diurnal variability of the surface NH_3 concentrations and are currently being further studied. The TES retrievals are corrected by subtracting mean biases. These biases are generated from the discrepancy between TES retrievals and true profiles [*Shephard et al.*, 2011], and the mean biases are calculated according to the type of the a priori profile (see Supplementary Figure 1).

A key aspect of inverse modeling is regularization through inclusion of the penalty, or background, term in the cost function. To define $\mathbf{S}_a$, uncertainties of ammonia in the emissions inventories are assumed to be 100% of the maximum emissions of ammonia across the globe. Uncertainties of SO_2 and NO_x are 20% and 50% of the maximum emission of corresponding sources across the globe. We also assume the errors are uncorrelated.

Using an L-curve selection criteria [*Hansen*, 1998] (see Supplementary Figure 2), we select the regularization parameter (γ) to be 124 for April, 100 for July, and 50 for October.

TES NH_3 observations are assimilated using the GEOS-Chem adjoint-based inversion. The total initial and optimized ammonia emissions are shown in Fig. 5. The initial model estimates of NH_3 profiles are predominately lower than the observations. The optimized emissions generally increase over the entire U.S.. There are large increases in southern California in all three months. Other large increases are located in the central U.S., as well as Mexico and Cuba. We do not have much information about NH_3 in Mexico and Cuba due to lack of measurement records there, but large (e.g. 15 ppb) NH_3 RVMR values are observed in April whereas the corresponding GEOS-Chem model estimates using the initial emissions are very small (e.g. 1.37 ppb). As a result of the inversion, emissions are increased in such areas by up to a factor of 9.

The RVMR represents a TES sensitivity weighted boundary layer averaged value with the influence of a priori reduced as much as possible [*Shephard et al.*, 2011]. We calculate RVMR only for retrievals that have high SNR and high thermal contrast. The RVMR is also calculated for the model in those locations which have valid TES retrievals. Fig. 6 shows the comparison of NH_3 RVMR from TES and GEOS-Chem before and after the assimilation. It has $500 \sim 700$ RVMR values in each month including values from 4 years. A linear fit of the model values to the observations is performed in each month, before and after optimization. The slope of this line increases in each month which indicates that most of the RVMR values from GEOS-Chem increase after the optimization. However, the modeled NH_3 RVMRs at low values change only slightly after the optimization in all three months. We note however that these differences in RVMR do not reflect observation bias

or uncertainty, which contribute to the cost function. In order to show the locations which have significant changes in RVMR, we consider spatial plots of the difference between the TES and GEOS-Chem RVMR before and after the assimilation for each month (Fig. 7). Initially, the model RVMRs are generally less than the TES RVMRs, as indicated by the blue points in the map. After the optimization, model RVMRs increase in many places. Some of the model RVMRs are larger than the TES RVMRs, as indicated by the red points in the map and the overall model bias relative to TES is reduced. The discrepancies of TES RVMRs and model RVMRs change from negative to positive in Southern California and Central U.S. in all three months, consistent with the spatial plots showing large increases of ammonia emissions in these locations (Fig. 5).

We next assess the sensitivity of these results to the assumed a priori emissions errors, $\mathbf{S}_a$. Table 1 shows the effects of varying a priori errors on the total optimized emissions of different species. We assume $\mathbf{S}_a(NH_3)$ to be 50% of the maximum a priori emission for all species. Generally, the results of the inversion are not very different in terms of total emission changes for each species from the base case inversion, see Table 1. However, absolute changes in total emissions of SO_2 and NO_x increase slightly as their uncertainties increase relative to those of NH_3, while changes in NH_3 total emissions decrease as uncertainty of NH_3 decreases.

6. Evaluation

In the next section, we compare model estimates using the optimized emissions to independent data sets not used during the inversion.

6.1. AMoN

We first consider a comparison of the posterior model results to AMoN NH_3 observations (Fig. 8). Initially, the model broadly underestimates AMoN values. After optimization, the NH_3 concentrations increase in each month. The R^2 increases by 22.4% in April, 28.9% in July and 27.2% in October. The slope increases by 353.3% in April, 96.1% in July and 77.1% in October. However, while the root mean square error (RMSE) decreases by 13% in April and 9.5% in October, it increases by 77.6% in July. The normalized mean bias (NMB) after the optimization decreases from -0.678 to -0.069 in April, increases from -0.045 and -0.138 to 0.659 and 0.166 in July and October, respectively. Overall, the model does a better job of capturing the range and variability of NH_3 at AMoN sites in April and October, while in July, the model estimates are consistently biased high.

TES has a detection limit of about 1 ppb, and a positive bias of about 0.5 ppb [*Shephard et al.*, 2011]. We can see model values that are below 1 ppb do not change significantly before and after the optimization in all three months (Fig. 8). The bias shown in Fig. 8 for July is much higher than 0.5 ppb. One possible reason may be the sampling bias of the TES retrievals. This can be assessed by analyzing NH_3 simulations from high resolution (12 km $\times$ 12 km) Community Multi-scale Air Quality (CMAQ) model simulations. Surface level NH_3 concentrations throughout the U.S. are compared to concentrations from locations corresponding to successful TES retrievals. The mean surface NH_3 concentration of CMAQ at locations which have successful TES retrievals is about 30% larger than the mean value of that for the whole U.S.. This comparison is facilitated by the fact that the TES footprint (5 km $\times$ 8 km) and CMAQ grid cells are similar in size. As shown in Fig. 8, changes in large concentrations drive the optimization. A lack of TES observations

329 constraining low values may allow for initial model values that already overestimate low
330 NH_3 concentrations to become even higher in the optimized model, because high TES
331 values, many of which are larger than the initial model estimate will dominate the cost
332 function. In future work, resampling the TES retrievals may be one way to decrease the
333 sampling bias. Increasing the model resolution may also improve our ability to model
334 localized peak NH_3 concentrations measured by TES and to match observations from
335 AMoN.

6.2. NTN

336 As an additional check of the broad NH_x budget, we consider the NH_x wet deposition
337 as recorded by NTN (NADP) sites. To make this comparison, we consider that simulated
338 precipitation is a critical driver in the performance of the GEOS-Chem simulated wet
339 deposition estimates, as biases in the model estimated precipitation can lead to biases
340 in the GEOS-Chem model estimates. We therefore adjust the modeled wet deposition
341 diagnostic to account for differences in the modeled and observed precipitation by linearly
342 scaling the model estimated wet deposition by the ratio of the observed to estimated
343 precipitation.

344 Figure 9 shows the comparison of modeled wet deposition with the NTN observations.
345 Generally, the inversion increases the wet deposition during all three months. Also corre-
346 lation (R^2) improves in each month. The square of correlation coefficient (R^2) increases by
347 30.6% in April, 393.9% in July and 27.9% in October. In July, optimized values increase
348 a lot; the slope of the linear regression line increases from 0.162 to 0.65, but in April and
349 October changes in NH_x wet deposition are not as significant as in July. Comparisons
350 between GEOS-Chem and NTN observations are also shown in *Zhang et al.* [2012]. They

compare the NH_3 wet deposition from GEOS-Chem at the $0.5°\times0.67°$ resolution with NTN observations from 2006. The emission inventories of NH_3 they use are different as anthropogenic sources of NH_3 are from NEI-2005 for U.S. with seasonal variability corrected by in situ observations. No significant annual biases and little seasonal bias are found in the comparison. Differences between this study and the present work are the model resolution, the number of months per season included in the comparisons (one vs three) and the emission inventories in the model. We will investigate using additional months and higher resolution inverse models as these become available.

6.3. IMPROVE

For an additional evaluation, we also compare the assimilated results with aerosol observations from IMPROVE in 2008. Figure 10 shows that model optimization slightly decreases the sulfate concentrations and increases the nitrate concentrations, which facilitates increases in NH_3 concentrations to match TES observations. Still, the changes are small, and the sulfate concentration from the model has a reasonable correlation with the IMPROVE observation before and after optimization in each month. Note that the outlier point in October that has a large observed value but a nearly zero model value is located in Hawaii. The model does not represent this high value owing to the proximity of the observation to the local volcano source. For nitrate, optimization does not help the comparison with the observations, which are initially too high. As modeled NH_3 increases to improve agreement with TES, leading to more nitrate formation, the model nitrate bias becomes even higher compared to IMPROVE. One hypothesis is that HNO_3 formation from N_2O_5 hydrolysis is too high in the model [*Zhang et al.*, 2012]. In contrast *Henze et al.* [2009] uses sulfate and nitrate to constrain the NH_3 emissions, which implies NH_3

sources are too high. Thus, to achieve closure relative to all data sets, it is evident that assessment of model error beyond NH_3 sources, in terms of scavenging efficiencies and HNO_3 production, is required.

7. Conclusions

Here we have considered the potential for space-based observations of NH_3 to constrain monthly average emissions factors. Initial tests using pseudo-observations show that under ideal conditions (i.e., a perfect model) using two-weeks worth of TES data, 70% of the variance of the emissions can be constrained in terms of total magnitude. We then proceed to assimilate TES observations for multiple years. Here, we present a range of constrained prediction results and evaluate them with independent data sets. Generally, model optimization increases NH_3 concentrations and NH_x wet deposition; nitrate and sulfate concentrations are not largely impacted. Overall, the model does a better job of capturing the range and variability of NH_3 at AMoN sites in April and October, while in July, the model estimates are consistently biased high. Compared to the wet deposition observations of NTN, optimization decreases the normalized mean bias (NMB) in April, enhances the NMB in July and October, but overall leads to increased correlation of modeled and observed values. Modeled SO_4^{2-} aerosol concentrations slightly decrease and NO_3^- aerosols concentrations increase, which increases the bias compare to the IMPROVE observation. The large NO_3^- aerosols concentrations may due to excessive HNO_3 formation in the model.

Overall, we conclude that inverse modeling with satellite information indeed helps constrain the ammonia emissions, particularly in strong source regions; additional observations or higher resolution inverse models may be necessary to constrain low values. The

findings indicate that the initial NH_3 emissions inventory appears to be broadly underestimated in several areas throughout the U.S., particularly in the west. This is at odds with previous inverse constraints based on nitrate aerosol alone [*Henze et al.*, 2009]. However, these results are consistent with more recent works regarding levels in the U.S. and globally [*Clarisse et al.*, 2009; *Zhang et al.*, 2012]. The absolute extent of the emissions underestimation is still in question, as the precise accuracy of the satellite observations is difficult to specify, model resolution is not matched to the satellite resolution, and model processes could have error contributing to uncertainty in the inversion. A greater fraction of peak values are included in the assimilation owing to satellite detection limits, leading to a sampling bias, which may cause the model to overestimate the emissions after optimization. Future work will be applying the model with a higher horizontal resolution (e.g. $0.5^\circ \times 0.67^\circ$). Also, consideration of bi-direcitonal flux of NH_3 may explain some of these results.

Acknowledgments. This work is supported by NASA grants NNX09AN77G and NNX10AG63G and EPA STAR award RD834559. While this manuscript has been reviewed by the Environmental Protection Agency and approved for publication, it may not reflect official agency views or policies.

References

Adams, P. J., J. H. Seinfeld, and D. M. Koch (1999), Global concentrations of tropospheric sulfate, nitrate, and ammonium aerosol simulated in a general circulation model, *J. Geophys. Res.*, *104*(D11), 13,791 – 13,823.

Aneja, V. P., J. P. Chauhan, and J. T. Walker (2000), Characterization of atmospheric ammonia emissions from swine waste storage and treatment lagoons, *J. Geophys. Res.*, *105*(D9), 11,535 – 11,545.

Aneja, V. P., W. H. Schlesinger, and J. W. Erisman (2008), Farming pollution, *Nature Geoscience*, *1*(7), 409–411, doi:10.1038/Ngeo236.

Beer, R., M. W. Shephard, S. Kulawik, S. A. Clough, R. A. Eldred, K. W. Bowman, S. P. Sander, B. M. Fisher, V. H. Payne, M. Louo, G. B. Osterman, and J. R. Worden (2008), First satellite observations of lower tropospheric ammonia and methanol, *Geophys. Res. Lett.*, *35*, L09801, doi:10.1029/2008GL033642.

Beusen, A. H. W., A. F. Bouwman, P. S. C. Heuberger, G. Van Drecht, and K. W. Van Der Hoek (2008), Bottom-up uncertainty estimates of global ammonia emissions from global agricultural production systems, *Atmos. Environ.*, *42*(24), 6067–6077.

Bey, I., D. J. Jacob, R. M. Yantosca, J. A. Logan, B. D. Field, A. M. Fiore, Q. B. Li, H. G. Y. Liu, L. J. Mickley, and M. G. Schultz (2001), Global modeling of tropospheric chemistry with assimilated meteorology: Model description and evaluation, *J. Geophys. Res.-Atmos.*, *106*(D19), 23,073–23,095.

Bouwman, A. F., D. S. Lee, W. A. H. Asman, F. J. Dentener, K. W. VanderHoek, and J. G. J. Olivier (1997), A global high-resolution emission inventory for ammonia, *Global Biogeochem. Cycles*, *11*, 561587.

Byrd, R. H., P. H. Lu, J. Nocedal, and C. Y. Zhu (1995), A limited memory algorithm for bound constrained optimization, *Siam J. Sci. Comput.*, *16*(5), 1190–1208.

Clarisse, L., C. Clerbaux, F. Dentener, D. Hurtmans, and P. F. Coheur (2009), Global ammonia distribution derived from infrared satellite observations, *Nature Geoscience*,

2(7), 479–483, doi:Doi 10.1038/Ngeo551.

Clarisse, L., M. W. Shephard, F. Dentener, D. Hurtmans, K. Cady-Pereira, F. Karagulian, M. Van Damme, C. Clerbaux, and P. F. Coheur (2010), Satellite monitoring of ammonia: A case study of the san joaquin valley, *J. Geophys. Res.-Atmos.*, *115*, D13302, doi: 10.1029/2009jd013291.

Dennis, R. L., P. V. Bhave, and R. W. Pinder (2008), Observable indicators of the sensitivity of $PM_{2.5}$ nitrate to emission reductions - Part II: Sensitivity to errors in total ammonia and total nitrate of the CMAQ-predicted non-linear effect of SO_2 emission reductions, *Atmos. Environ.*, *42*(6), 1287–1300, doi:10.1016/J.Atmosenv.2007.10.036.

Duncan, B. N., R. V. Martin, A. C. Staudt, R. Yevich, and J. A. Logan (2003), Interannual and seasonal variability of biomass burning emissions constrained by satellite observations, *J. Geophys. Res.-Atmos.*, *108*(D2), doi:10.1029/2002JD002378.

Galloway, J. N., A. R. Townsend, J. W. Erisman, M. Bekunda, Z. C. Cai, J. R. Freney, L. A. Martinelli, S. P. Seitzinger, and M. A. Sutton (2008), Transformation of the nitrogen cycle: Recent trends, questions, and potential solutions, *Science*, *320*(5878), 889–892, doi:10.1126/Science.1136674.

Gilliland, A. B., R. L. Dennis, S. J. Roselle, and T. E. Pierce (2003), Seasonal NH_3 emission estimates for the eastern United States based on ammonium wet concentrations and an inverse modeling method, *J. Geophys. Res.-Atmos.*, *108*(D15), 4477, doi: 10.1029/2002JD003063.

Gilliland, A. B., K. W. Appel, R. W. Pinder, and R. L. Dennis (2006), Seasonal NH_3 emissions for the continental United States: Inverse model estimation and evaluation, *Atmos. Environ.*, *40*(26), 4986–4998.

461 Hansen, P. (1998), *Rank-Deficient and Discrete Ill-Posed Problems: Numerical Aspects of*
462 *Linear Inversion.*, Society for Industrial Mathematics, PA, USA.

463 Heald, C. L., D. J. Jacob, R. J. Park, L. M. Russell, B. J. Huebert, J. H. Seinfeld, H. Liao,
464 and R. J. Weber (2005), A large organic aerosol source in the free troposphere missing
465 from current models, *Geophys. Res. Lett.*, *32*, L18809, doi:10.1029/2005GL023831.

466 Heald, C. L., D. J. Jacob, S. Turquety, R. C. Hudman, R. J. Weber, A. P. Sullivan,
467 R. E. Peltier, E. L. Atlas, J. A. de Gouw, C. Warneke, J. S. Holloway, J. A. Neu-
468 man, F. M. Flocke, and J. H. Seinfeld (2006), Concentrations and sources of organic
469 carbon aerosols in the free troposphere over North America, *J. Geophys. Res.-Atmos.*,
470 *111*(D23), D23S47, doi:10.1029/2006JD007705.

471 Henze, D. K., A. Hakami, and J. H. Seinfeld (2007), Development of the adjoint of GEOS-
472 Chem, *Atmos. Chem. Phys.*, *7*, 2413–2433.

473 Henze, D. K., J. H. Seinfeld, and D. Shindell (2009), Inverse modeling and mapping
474 U.S. air quality influences of inorganic $PM_{2.5}$ precursor emissions using the adjoint of
475 geos-chem, *Atmos. Chem. Phys.*, *9*, 5877–5903.

476 Liao, H., D. K. Henze, J. H. Seinfeld, S. Wu, and L. J. Mickley (2007), Biogenic secondary
477 organic aerosol over the United States: Comparison of climatological simulations with
478 observations, *J. Geophys. Res.-Atmos.*, *112*, D06201, doi:10.1029/2006JD007813.

479 Malm, W. C., B. A. Schichtel, M. L. Pitchford, L. L. Ashbaugh, and R. A. Eldred (2004),
480 Spatial and monthly trends in speciated fine particle concentration in the United States,
481 *J. Geophys. Res.-Atmos.*, *109*(D3), D03306, doi:10.1029/2003jd003739.

482 Nowak, J. B., L. G. Huey, A. G. Russell, D. Tian, J. A. Neuman, D. Orsini, S. J. Sjost-
483 edt, A. P. Sullivan, D. J. Tanner, R. J. Weber, A. Nenes, E. Edgerton, and F. C.

Fehsenfeld (2006), Analysis of urban gas phase ammonia measurements from the 2002 Atlanta Aerosol Nucleation and Real-Time Characterization Experiment (ANARChE), *J. Geophys. Res.-Atmos.*, *111*(D17), D17308, doi:10.1029/2006JD007113.

Park, R. J., D. Jacob, B. D. Field, R. Yantosca, and M. Chin (2004), Natural and transboundary pollution influences on sulfate-nitrate-ammonium aerosols in the United States: Implications for policy, *J. Geophys. Res.-Atmos.*, *109*, D15204, doi: 10.1029/2003JD004473.

Park, R. J., D. J. Jacob, N. Kumar, and R. M. Yantosca (2006), Regional visibility statistics in the United States: Natural and transboundary pollution influences, and implications for the Regional Haze Rule, *Atmos. Environ.*, *40*(28), 5405–5423.

Payne, V. H., S. A. Clough, M. W. Shephard, R. Nassar, and J. A. Logan (2009), Information-centered representation of retrievals with limited degrees of freedom for signal: Application to methane from the tropospheric emission spectrometer, *J. Geophys. Res.*, doi:10.1029/2008JD010155.

Pinder, R. W., P. J. Adams, S. N. Pandis, and A. B. Gilliland (2006), Temporally resolved ammonia emission inventories: Current estimates, evaluation tools, and measurement needs, *J. Geophys. Res.-Atmos.*, *111*(D16), D16310, doi:10.1029/2005JD006603.

Pinder, R. W., J. T. Walker, J. O. Bash, K. E. Cady-Pereira, D. K. Henze, M. Luo, G. B. Osterman, and M. W. Shephard (2011), Quantifying spatial and temporal variability in atmospheric ammonia with in situ and space-based observations, *Geophys. Res. Lett.*, *38*, doi:Doi 10.1029/2010GL046146.

Pope, C. A., R. T. Burnett, M. J. Thun, E. E. Calle, D. Krewski, K. Ito, and G. D. Thurston (2002), Lung cancer, cardiopulmonary mortality, and long-term exposure to

fine particulate air pollution, *J. Am. Med. Assoc.*, *287*(9), 1132–1141.

Pye, H. O. T., H. Liao, S. Wu, L. J. Mickley, D. J. Jacob, D. K. Henze, and J. H. Seinfeld (2009), Effets of changes in climate and emissions on future sulfate-nitrate-ammonium aerosol levels in the United States, *J. Geophys. Res.-Atmos.*, *114*, D01205, doi:10.1029/2008JD010701.

Rabalais, N. N. (2002), Nitrogen in aquatic ecosystems, *Ambio*, *31*(2), 102–112.

Reiss, R., E. L. Anderson, C. E. Cross, G. Hidy, D. Hoel, R. McClellan, and S. Moolgavkar (2007), Evidence of health impacts of sulfate- and nitrate-containing particles in ambient air, *Inhal Toxicol*, *19*(5), 419–449, doi:10.1080/08958370601174941.

Rodgers, C. D. (2000), *Inverse Methods for Atmospheric Sounding*, *Series on Atmospheric, Oceanic and Planetary Physics*, vol. 2, World Scientific, Singapore.

Rodhe, H., F. Dentener, and M. Schulz (2002), The global distribution of acidifying wet deposition, *Environ. Sci. Technol.*, *36*(20), 4382–4388, doi:10.1021/Es020057g.

Roelle, P. A., and V. P. Aneja (2002), Characterization of ammonia emissions from soils in the upper coastal plain, north carolina, *Atmos. Environ.*, *36*, 1087 – 1097.

Sandu, A., D. N. Daescu, G. R. Carmichael, and T. F. Chai (2005), Adjoint sensitivity analysis of regional air quality models, *J. Comput. Phys.*, *204*(1), 222–252.

Schlesinger, W. H. (2009), On the fate of anthropogenic nitrogen, *Proc. Natl. Acad. Sci. U. S. A.*, *106*(1), 203–208, doi:10.1073/Pnas.0810193105.

Schoeberl, M. R., A. R. Douglass, E. Hilsenrath, P. K. Bhartia, R. Beer, J. W. Waters, M. R. Gunson, L. Froidevaux, J. C. Gille, J. J. Barnett, P. E. Levelt, and P. DeCola (2006), Overview of the EOS Aura mission, *Ieee Transactions on Geoscience and Remote Sensing*, *44*(5), 1066–1074, doi:10.1109/Tgrs.2005.861950.

Schwartz, J., F. Laden, and A. Zanobetti (2002), The concentration-response relation between $PM_{2.5}$ and daily deaths, *Environ. Health Perspect.*, *110*(10), 1025–1029.

Shephard, M. W., H. M. Worden, K. E. Cady-Pereira, M. Lampel, M. Z. Luo, K. W. Bowman, E. Sarkissian, R. Beer, D. M. Rider, D. C. Tobin, H. E. Revercomb, B. M. Fisher, D. Tremblay, S. A. Clough, G. B. Osterman, and M. Gunson (2008), Tropospheric emission spectrometer nadir spectral radiance comparisons, *J. Geophys. Res.-Atmos.*, *113*(D15), D15S05, doi:10.1029/2007jd008856.

Shephard, M. W., K. E. Cady-Pereira, M. Luo, D. K. Henze, R. W. Pinder, J. T. Walker, C. P. Rinsland, J. O. Bash, L. Zhu, V. H. Payne, and L. Clarisse (2011), TES ammonia retrieval strategy and global observations of the spatial and seasonal variabiity of ammonia, *Atmos. Chem. Phys.*, *11*(5), 16,023–16,074.

Simon, H., D. T. Allen, and A. E. Wittig (2008), Fine particulate matter emissions inventories: Comparisons of emissions estimates with observations from recent field programs, *J. Air Waste Manage. Assoc.*, *58*(2), 320–343, doi:10.3155/1047-3289.58.2.320.

Stephen, K., and V. P. Aneja (2008), Trends in agricultural ammonia emissions and ammonium concentrations in precipitation over the Southeast and Midwest United States, *Atmos. Environ.*, *42*(14), 3238–3252.

Sutton, M. A., E. Nemitz, J. W. Erisman, C. Beier, K. B. Bahl, P. Cellier, W. de Vries, F. Cotrufo, U. Skiba, C. Di Marco, S. Jones, P. Laville, J. F. Soussana, B. Loubet, M. Twigg, D. Famulari, J. Whitehead, M. W. Gallagher, A. Neftel, C. R. Flechard, B. Herrmann, P. L. Calanca, J. K. Schjoerring, U. Daemmgen, L. Horvath, Y. S. Tang, B. A. Emmett, A. Tietema, J. Penuelas, M. Kesik, N. Brueggemann, K. Pilegaard, T. Vesala, C. L. Campbell, J. E. Olesen, U. Dragosits, M. R.

553 Theobald, P. Levy, D. C. Mobbs, R. Milne, N. Viovy, N. Vuichard, J. U. Smith,
554 P. Smith, P. Bergamaschi, D. Fowler, and S. Reis (2007), Challenges in quantifying
555 biosphere-atmosphere exchange of nitrogen species, *Environ. Pollut.*, *150*(1), 125–139,
556 doi:10.1016/J.Envpol.2007.04.014.

557 Wu, S.-Y., J.-L. Hu, Y. Zhang, and V. P. Aneja (2008), Modeling atmospheric transport
558 and fate of ammonia in North Carolina–Part II: Effect of ammonia emissions on fine
559 particulate matter formation, *Atmos. Environ.*, *42*(14), 3437–3451.

560 Yevich, R., and J. A. Logan (2003), An assessment of biofuel use and burning of agri-
561 cultural waste in the developing world, *Global Biogeochem. Cycles*, *17*(4), 1095, doi:
562 10.1029/2002GB001952.

563 Yu, S. C., R. Dennis, S. Roselle, A. Nenes, J. Walker, B. Eder, K. Schere, J. Swall, and
564 W. Robarge (2005), An assessment of the ability of three-dimensional air quality models
565 with current thermodynamic equilibrium models to predict aerosol NO3$^-$, *J. Geophys.*
566 *Res.-Atmos.*, *110*(D7), D07S13, doi:10.1029/2004jd004718.

567 Zhang, L., D. J. Jacob, E. M. Knipping, N. Kumar, J. W. Munger, C. C. Carouge, A. van
568 Donkelaar, Y. X. Wang, and D. Chen (2012), Nitrogen deposition to the united states:
569 distribution, sources, and processes, *Atmospheric Chemistry and Physics Discussions*,
570 *12*(1), 241–282, doi:10.5194/acpd-12-241-2012.

571 Zhang, Y., S.-Y. Wu, S. Krishnan, K. Wang, A. Queen, V. P. Aneja, and S. P. Arya (2008),
572 Modeling agricultural air quality: Current status, major challenges, and outlook, *Atmos.*
573 *Environ.*, *42*(14), 3218–3237.

574 Zhu, C., R. H. Byrd, P. Lu, and J. Nocedal (1994), L-BFGS-B: A limited memory FOR-
575 TRAN code for solving bound constrained optimization problems, *Tech. rep.*, North-

western University.

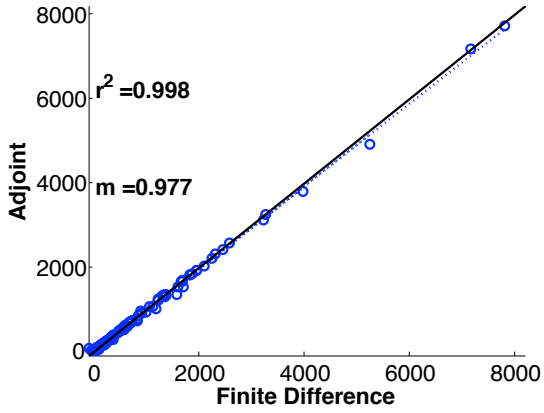

Figure 1. Validation of adjoint model sensitivities via comparison to finite difference (FD) results for week-long simulations. Solid lines are 1:1, dashed are regressions with given r^2 and slope m.

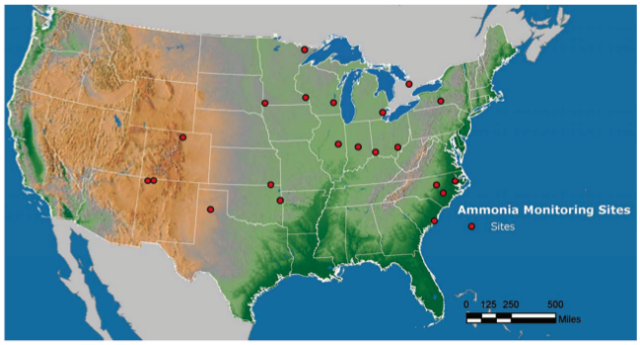

Figure 2. Monitoring sites locations for the Ammonia Monitoring Network (AMoN).

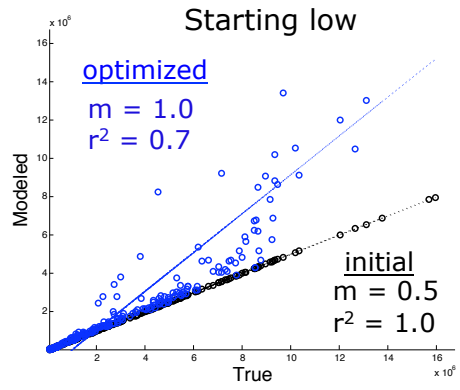

(a)

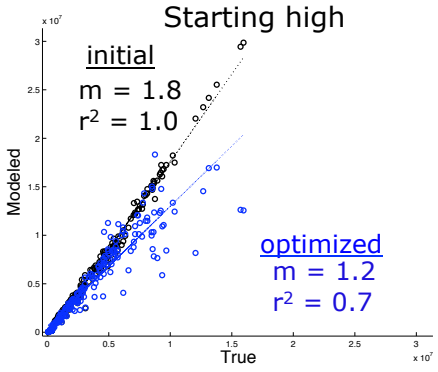

(b)

Figure 3. Emissions before (initial) and after (optimized) inversions using TES pseudo observations. To test the inverse model, NH_3 emissions were initialized to values different than the true emissions. In panel (a), the initial emissions are half the true values; in (b), the initial emissions are 1.8 times the true values.

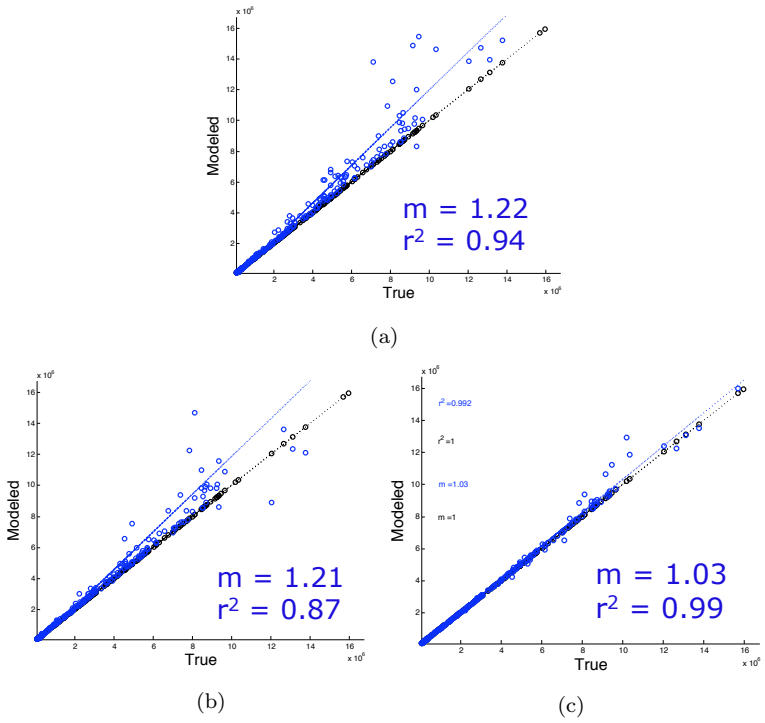

Figure 4. Tests for the possible impacts of inversion error, retrieval bias and measurement error: (a) retrieval algorithm with a polluted profile as an initial guess; (b) modified retrieval algorithm with a moderate profile as the initial guess; (c) model profiles from the true model were ascribed error of the same size as the measurement error.

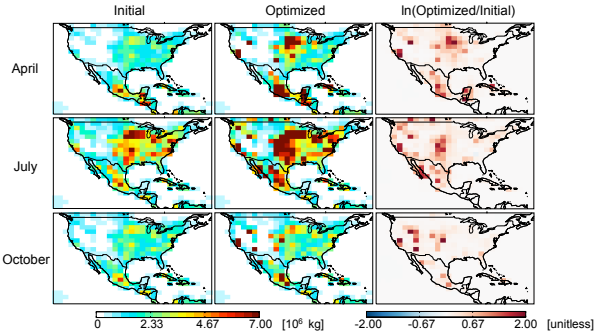

Figure 5. NH_3 emissions from GEOS-Chem before and after the assimilation.

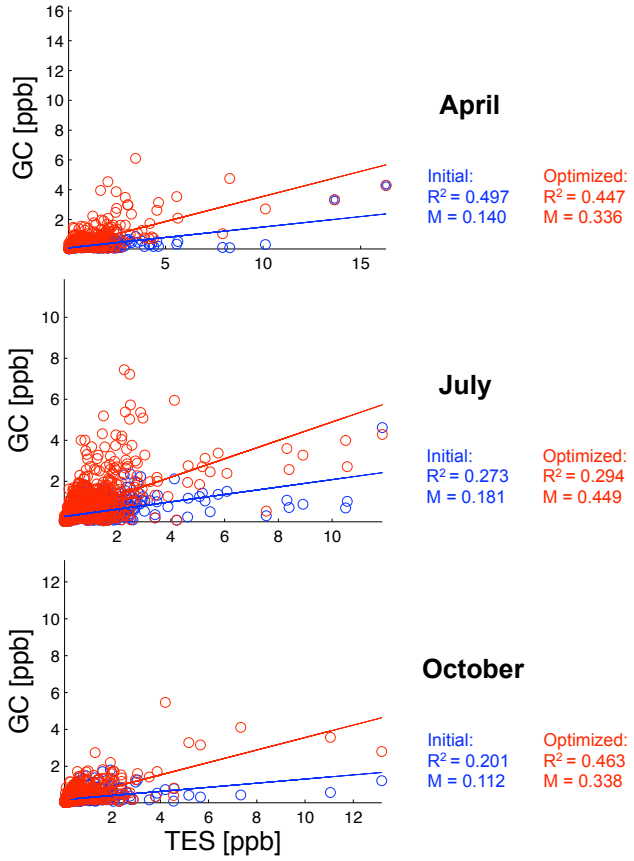

Figure 6. Comparison of NH_3 Representative volume Mixing Ratio (RVMR) from TES and GEOS-Chem before and after the assimilation.

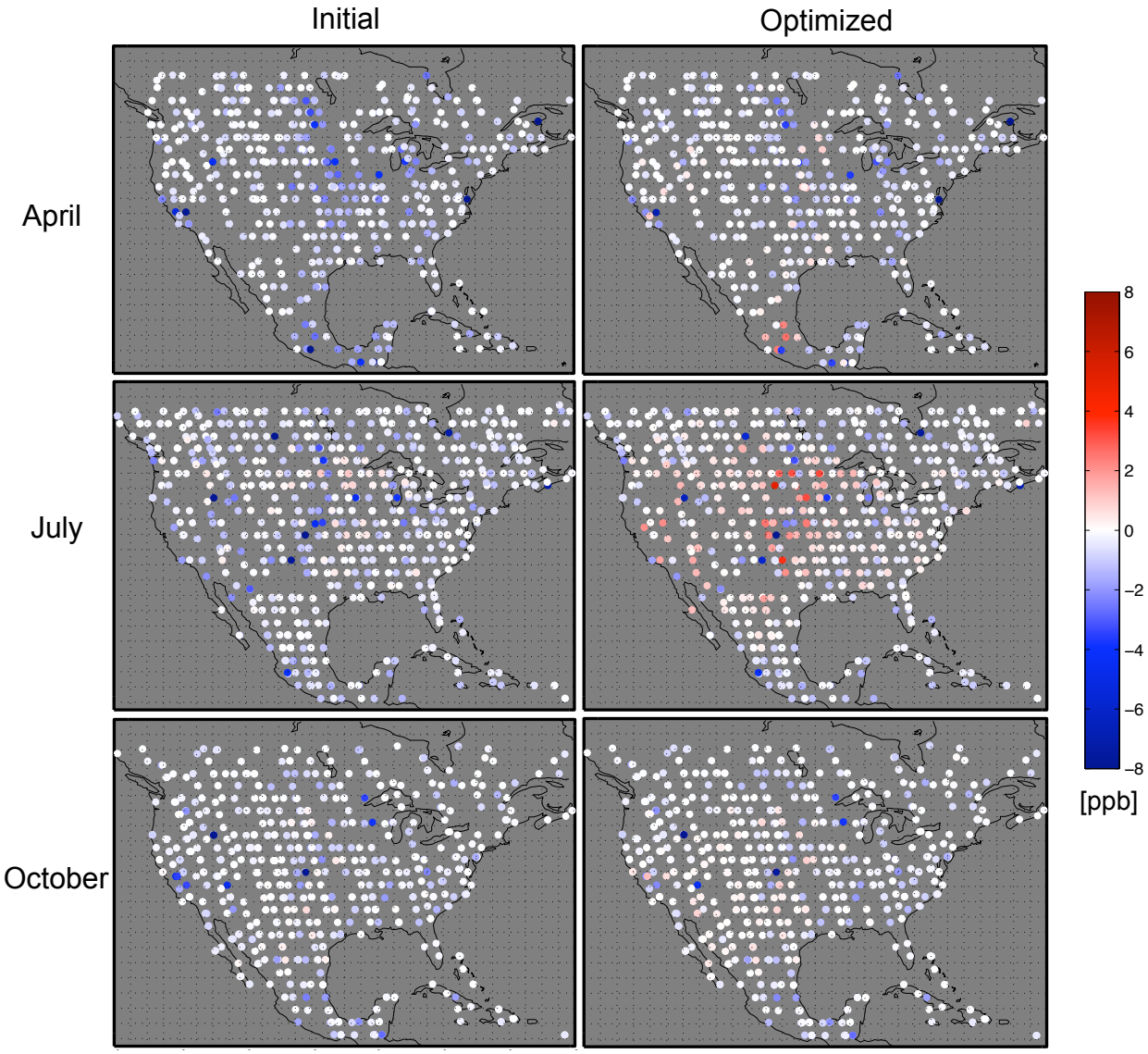

Figure 7. Difference of NH_3 Representative volume Mixing Ratio (RVMR) between TES and GEOS-Chem before and after the assimilation. The left column shows GEOS-Chem initial RVMR - TES RVMR; the right column shows GEOS-Chem optimized RVMR - TES RVMR.

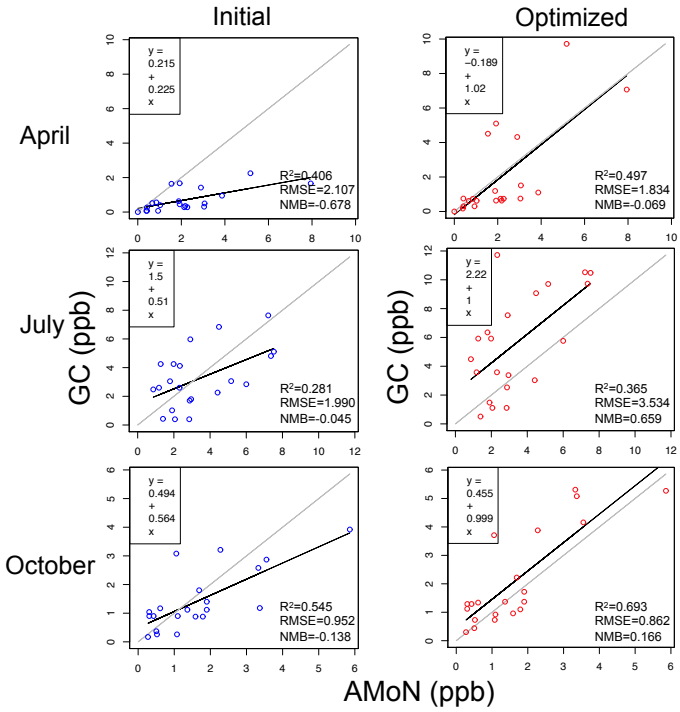

Figure 8. Comparison of GEOS-Chem NH_3 concentrations with observations from AMoN sites before and after the assimilation. The square of the correlation coefficient (R^2), root mean square error (RMSE), and normalized mean bias (NMB) are shown. Black solid lines are regressions. Grey dashed lines are 1:1.

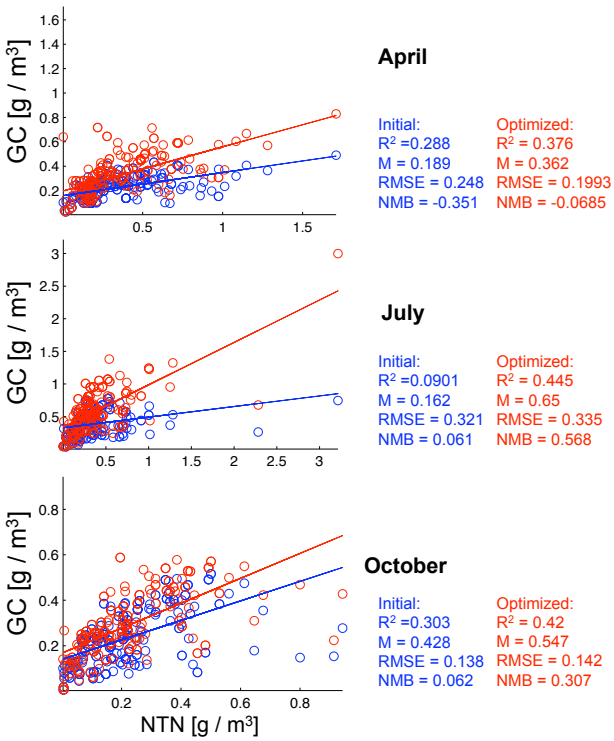

Figure 9. Comparison of GEOS-Chem NH_x wet deposition with observations from NTN(NADP) sites before and after the assimilation.

Table 1. The effects of a priori error emissions ($\mathbf{S}_a$) on the optimized emissions of different species. Total emissions changes in the U.S. for NH_3, NO_x, and SO_2 when using different values for the diagonal of $\mathbf{S}_a$ in the optimization. E^0 is the initial emissions.

Month	Uncertainties, $\mathbf{S}_a/MAX(E^0)$	Total emissions changes
	SO_2 NO_x NH_3	ΔSO_2 ΔNO_x ΔNH_3
April	20% 50% 100%	-11.9% -14.69% 112.99%
	50% 50% 50%	-11.58% -15.39% 99.95%
July	20% 50% 100%	-8.35% -4.24% 54.80%
	50% 50% 50%	-10.23% -4.58% 53.26%
October	20% 50% 100%	-3.56% -1.99% 36.07%
	50% 50% 50%	-3.64% -2.41% 35.16%

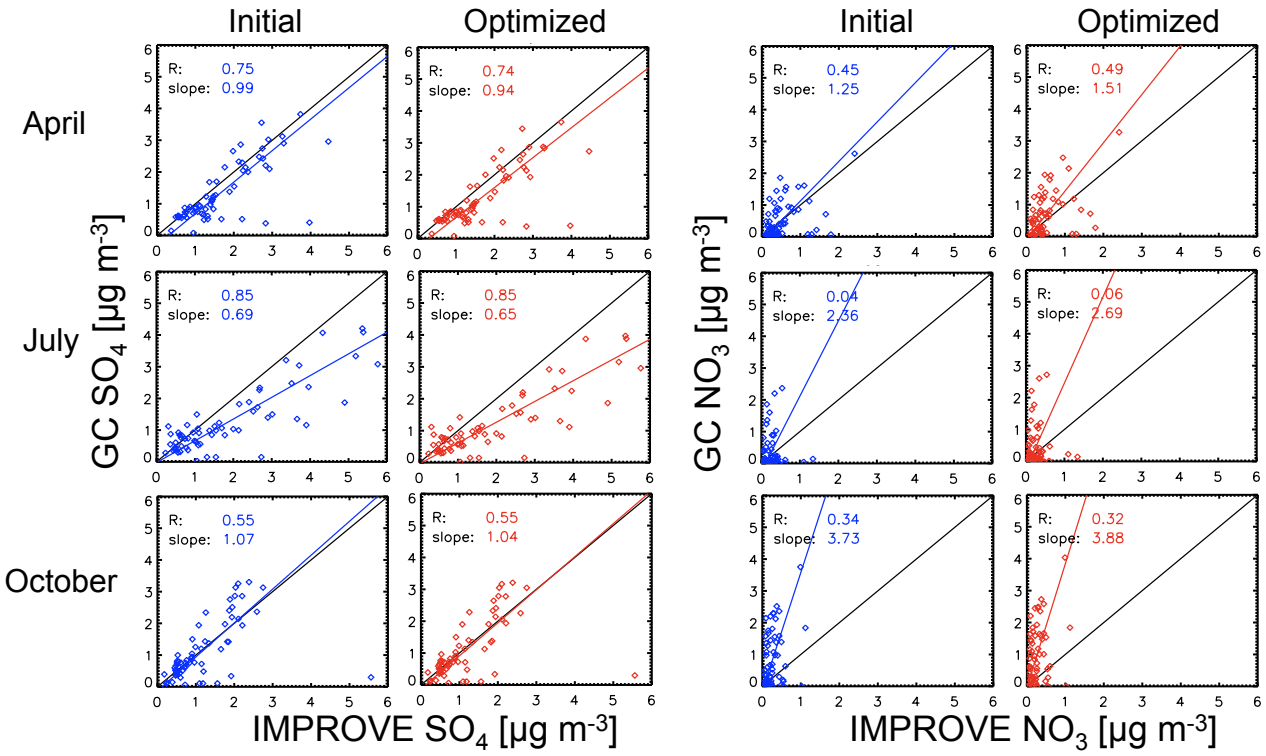

Figure 10. Comparison of GEOS-Chem SO_4 and NO_3 concentrations with observations from IMPROVE sites before and after the assimilation.

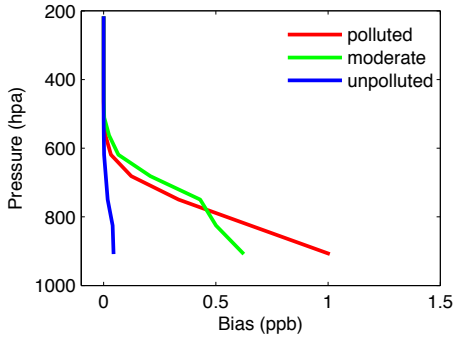

Supplementary Figure 1. The average discrepancy between TES retrievals and true profiles [*Shephard et al.*, 2011]. The mean biases are calculated according to the type of the a priori profile used in the retrieval.

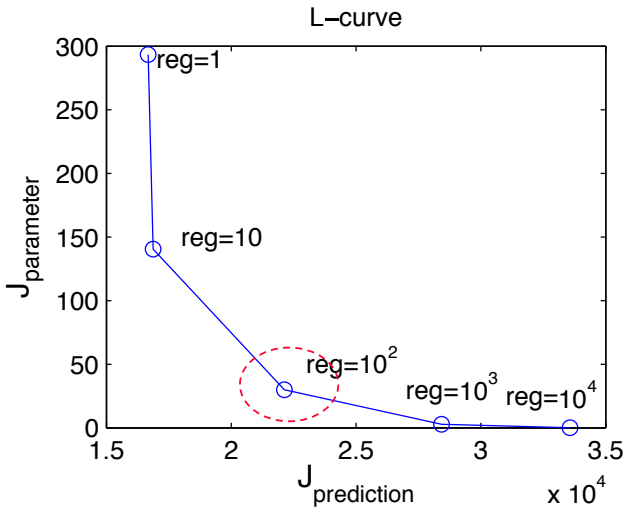

Supplementary Figure 2. The L-curve plot used for selecting the regularization parameter (γ) in July. $J_{parameter} = \frac{1}{2}\sum_{\mathbf{c}\in\Omega}(H\mathbf{c} - (\mathbf{c}_{obs} - \mathbf{b}))^T\mathbf{S}_{obs}^{-1}(H\mathbf{c} - (\mathbf{c}_{obs} - \mathbf{b}))$. $J_{prediction} = \frac{1}{2}(\boldsymbol{\sigma} - \boldsymbol{\sigma}_a)^T\mathbf{S}_a^{-1}(\boldsymbol{\sigma} - \boldsymbol{\sigma}_a)$. We select γ to be 100 in this case.